

High-Performance Red-Light Photodetector Based on Lead-Free Bismuth Halide Perovskite Film

Xiao-Wei Tong,[†] Wei-Yu Kong,[§] You-Yi Wang,[§] Jin-Miao Zhu,^{‡,*} Lin-Bao Luo,^{§,*} and Zheng-Hua Wang^{†,*}

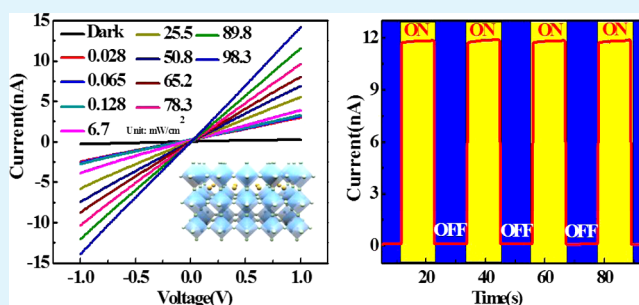
[†]Key Laboratory of Functional Molecular Solids, Ministry of Education, College of Chemistry and Materials Science, Anhui Normal University, Wuhu 241000, China

[‡]Department of Chemistry and Chemical Engineering, Hefei Normal University, Hefei 230061, China

[§]School of Electronic Sciences and Applied Physics, Hefei University of Technology, Hefei 230009, China

ABSTRACT: In this study, we developed a sensitive red-light photodetector (RLPD) based on CsBi₃I₁₀ perovskite thin film. This inorganic, lead-free perovskite was fabricated by a simple spin-coating method. Device analysis reveals that the as-assembled RLPD was very sensitive to 650 nm light, with an on/off ratio as high as 10⁵. The responsivity and specific detectivity of the device were estimated to be 21.8 A/W and 1.93 × 10¹³ Jones, respectively, which are much better than those of other lead halide perovskite devices. In addition, the device shows a fast response (rise time: 0.33 ms; fall time: 0.38 ms) and a high external quantum efficiency (4.13 × 10³%). It is also revealed that the RLPD has a very good device stability even after storage for 3 months under ambient conditions. In summary, we suggest that the CsBi₃I₁₀ perovskite photodetector developed in this study may have potential applications in future optoelectronic systems.

KEYWORDS: photodetector, lead-free, inorganic perovskite, responsivity, specific detectivity



INTRODUCTION

Since the publication of the first report on perovskite solar cells in 2009,^{1,2} methylammonium lead halide (e.g., CH₃NH₃PbX₃; X = Cl, Br, I) perovskite materials have received huge research interest worldwide because of their tunable direct band gap, high carrier mobility, and large absorption coefficient.³ In addition to photovoltaic devices, methylammonium lead halide materials in the form of either thin films, nanocrystals, or nanowires have been demonstrated to be ideal candidates for assembling other electronic and optoelectronic devices, such as photodetectors,^{4–7} chemical sensors,^{8,9} light-emitting diodes,^{10–13} and lasers.^{14–16} Among these perovskite-based devices, photodetectors, which can directly convert light illumination into electrical signal, are of particular importance for their promising application not only in military fields, such as target detection, military surveillance, and space-based warning, but also in civil fields, including light vision, remote control, industry automation control, and nondestructive image technology. Because of these merits, a number of perovskite photodetectors with high performance have been developed. For example, Cho's group developed a novel hybrid photodetector composed of CH₃NH₃PbI₃ layers and graphene. Owing to the unique absorption and the photogating mechanism of the heterojunction, the perovskite–graphene hybrid photodetector exhibited a high specific detectivity of ~10⁹ Jones.¹⁷ Hu et al. fabricated a flexible CH₃NH₃PbI₃-film-

based broad-band photodetector. The as-assembled organic halide lead perovskite photodetector exhibited obvious sensitivity to a broad-band wavelength from visible light to ultraviolet light. At 780 and 365 nm, the device had responsivities of 0.0367 and 3.49 A/W and external quantum efficiencies (EQEs) of 5.84 and 1.19 × 10³%.¹⁸ By using a simple solution-processed method, Yang's group reported a high-performance organic–inorganic hybrid perovskite photodetector. The device, using CH₃NH₃PbI_{3–x}Cl_x layer as light harvester, displayed a large specific detectivity, approaching 10 Jones,¹⁴ and a fast photoresponse of up to 3 MHz with 3 dB bandwidth.¹⁹ In spite of these progresses, the above perovskite-based photodetectors have two obvious problems: first, because of the presence of Pb atoms, which are environmentally unfriendly substances, the application of these devices is strictly prohibited. Second, the methylammonium is not stable. As a result, the methylammonium lead halide perovskite-based photodetectors usually have low ambient device stability. To address this problem, various groups have tried to substitute the Pb with Ge,²⁰ Mn,²¹ and Sn.²² Unfortunately, the as-substituted perovskite materials still have some shortcomings, such as poor device performance,²³ high cost,²⁰ and toxicity.²⁴ In this study,

Received: March 31, 2017

Accepted: May 16, 2017

Published: May 16, 2017

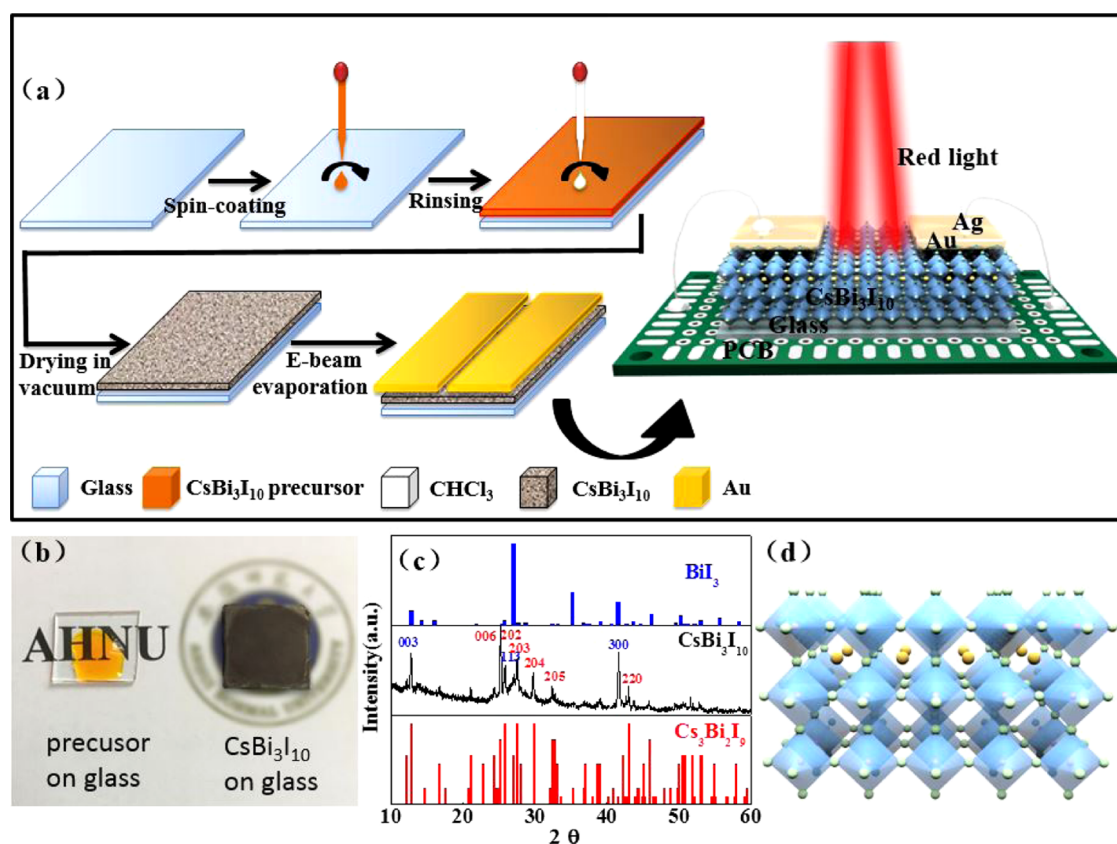


Figure 1. (a) Schematic illustration of the stepwise process for the fabrication of the CsBi₃I₁₀ perovskite film photodetector. (b) Picture of both the precursor and the CsBi₃I₁₀ perovskite film on glass. (c) XRD pattern of the CsBi₃I₁₀ perovskite film. (d) Schematic illustration of the crystal structure of the CsBi₃I₁₀ perovskite film; the purple, green, and yellow spheres represent Bi, I, and Cs atoms, respectively.

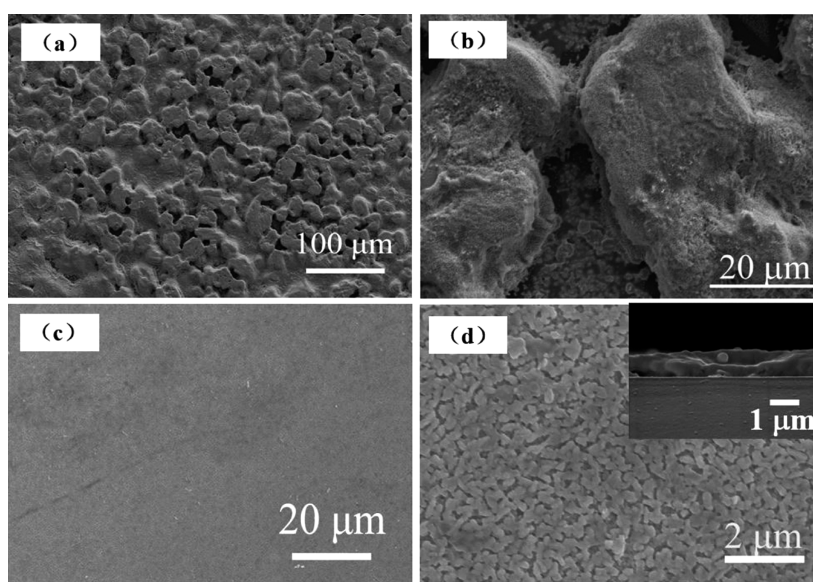


Figure 2. FESEM images of the CsBi₃I₁₀ perovskite film obtained via direct spin coating at low magnification (a) and high magnification (b). FESEM images of the CsBi₃I₁₀ perovskite film after NCP and VFSP treatments at low magnification (c) and high magnification (d), in which the inset shows the cross-sectional SEM image of the film on Si.

we report on the fabrication of a new inorganic, lead-free perovskite red-light photodetector (RLPD). The CsBi₃I₁₀ perovskite film was synthesized by a simple spin-coating method. Optoelectronic study revealed that the as-assembled device exhibited obvious sensitivity to red-light illumination, with excellent reproducibility and good spectral selectivity.

Under 650 nm illumination, the responsivity and specific detectivity of the device were estimated to be 21.8 A/W and 1.93×10^{13} Jones, respectively. Furthermore, the perovskite photodetector has a high response speed of <1 ms ($t_{\text{rise}}/t_{\text{fall}} = 0.33/0.38$). The above result confirms that the present CsBi₃I₁₀

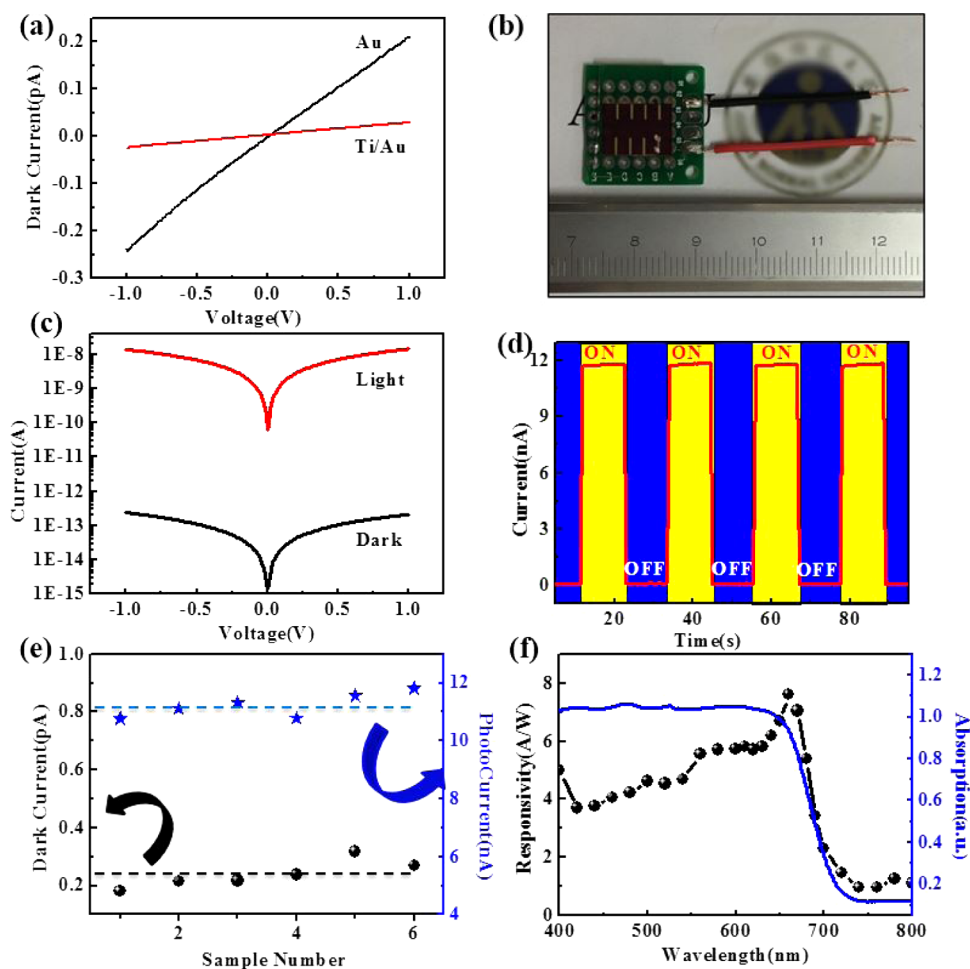


Figure 3. (a) Typical I – V characteristics of the RLPD with different metal electrodes. (b) Picture of the RLPD. (c) Typical I – V characteristics of the PD with Au electrodes under light and in dark at log scale. (d) Photoresponse of the RLPD when the 650 nm light was alternately turned on and off at +1 V bias voltage. (e) Dark current and photocurrent of six typical $\text{CsBi}_3\text{I}_{10}$ -film-based RLPDs. (f) Comparison of the absorption of the $\text{CsBi}_3\text{I}_{10}$ film and the spectral selectivity of the $\text{CsBi}_3\text{I}_{10}$ -film-based RLPD.

film photodetector may have potential applications in future optoelectronic device systems.

RESULTS AND DISCUSSION

Figure 1a illustrates the stepwise procedure to fabricate the lead-free perovskite-film-based RLPD. The $\text{CsBi}_3\text{I}_{10}$ perovskite film was fabricated by directly spin-coating the precursor on glass through a modified spin-coating method, which has been reported previously.²⁵ After synthesis, the brownish black, inorganic, lead-free perovskite film on glass (Figure 1b) was deposited by two metal electrodes (Au: 50 nm), with the assistance of a shadow mask. The as-assembled device was then placed on a printed circuit board (PCB). For the sake of stability, aluminum wires (5 μm) were then used to connect the two Ti/Au electrodes to the PCB through wire bonding. To study the phase of the perovskite film, the X-ray diffraction (XRD) pattern was then studied. As shown in Figure 1c, all of the diffraction peaks can be readily ascribed to the rhombohedral structure of BiI_3 , with lattice constants $a = 0.75$ nm and $c = 2.07$ nm, and the hexagonal structure of $\text{Cs}_3\text{Bi}_2\text{I}_9$, with lattice constants $a = 0.84$ nm and $c = 2.1$ nm. According to previous study,²⁵ like BiI_3 , the present $\text{CsBi}_3\text{I}_{10}$ has a layered crystal structure, which is partially broken into a

zero-dimensional structure as in $\text{Cs}_3\text{Bi}_2\text{I}_9$ between the layers (Figure 1d).

It should be pointed out that during the synthesis of the $\text{CsBi}_3\text{I}_{10}$ perovskite film chloroform was used to accelerate the volatilization of the solvent [dimethylformamide (DMF) and dimethyl sulfoxide (DMSO)], followed by drying under vacuum condition. Such a nanocrystal pinning (NCP)²⁶ and vacuum-flash-assisted solution process²⁷ (VFSP) are highly beneficial to the growth of high-quality thin films. Figure 2a–d compares the field emission scanning electron microscopy (FESEM) images of the $\text{CsBi}_3\text{I}_{10}$ perovskite film with and without further NCP and VFSP treatments. It is clear that the thin films obtained directly from spin coating are composed of large particles. However, the product after NCP and VFSP treatments has a highly smooth thin film.

To select an ideal electrode metal for the photodetector, we deposited both Au and Ti/Au electrodes with different work functions on the perovskite material. Figure 3a shows the I – V curves of a 1 μm thick $\text{CsBi}_3\text{I}_{10}$ film with different electrodes. It was found that the electrical conductivity of Au/ $\text{CsBi}_3\text{I}_{10}$ /Au is 1 order of magnitude larger than that of Au/Ti/ $\text{CsBi}_3\text{I}_{10}$ /Ti/Au, indicating the relatively low contact resistance of the Au/ $\text{CsBi}_3\text{I}_{10}$ interface. This finding is consistent with the fact that the perovskite material usually exhibits a weak p-type electrical conductivity,⁵ which needs a metal electrode with a relatively

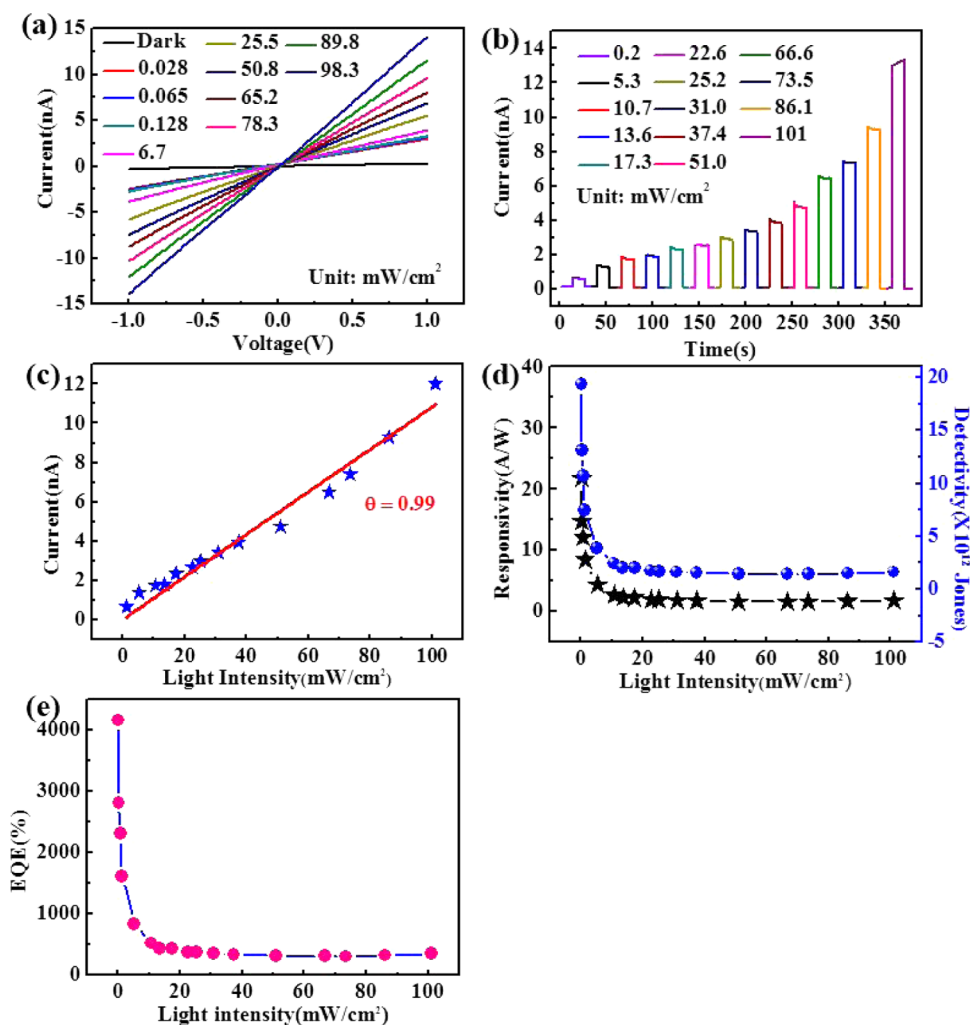


Figure 4. (a) Typical I - V characteristics of the CsBi₃I₁₀ RLPD under different intensities of illumination of 650 nm light. (b) The corresponding photoresponse of the RLPD under the 650 nm light with various power intensities at +1 V bias voltage. (c) The fitting of the relationship between the photocurrent and intensity. (d) The responsivity and specific detectivity as a function of light intensity. (e) The EQE as a function of light intensity.

high work function for Ohmic contact. In light of this, Au electrodes were used to fabricate the photodetector (Figure 3b). Interestingly, once the Au/CsBi₃I₁₀/Au-based photodetector was shined by 650 nm light, it will display pronounced photoresponse. As shown in Figure 3c,d, at a bias voltage of 1 V, the dark current is as low as 0.16 pA; however, the photocurrent is as high as 11.8 nA under light illumination, with an intensity of 84 mW/cm², yielding an on/off ratio as high as 10⁵. Besides the high on/off ratio, the photoresponse of the present CsBi₃I₁₀ RLPD is highly reproducible: the device can be easily switched between high-conductivity and low-conductivity states when the incident light was repeatedly turned on and off. Figure 3e shows both the dark current and photocurrent of six representative perovskite photodetectors, with two straight lines denoting the average values. It was observed that the majority of the devices show a dark current in the range of 0.16–0.31 pA, with an average value of 0.24 pA, and a photocurrent in the range of 10.7–11.8 nA, with an average value of 11.3 nA. It is worth noting that the present device shows excellent spectral selectivity. Figure 3f shows the spectral photoresponse in the wavelength range of 400–800 nm. Obviously, the RLPD was sensitive to light illumination with wavelength less than 650 nm. Nevertheless, it was virtually

blind to light illumination with wavelength longer than 700 nm. This good spectral selectivity is in agreement with the absorption curve, according to which, the band gap of the CsBi₃I₁₀ material is estimated to be 1.77 eV.²⁵ Understandably, the peak photosensitivity at 650 nm is associated with the trade-off between the number of photogenerated carriers and the kinetic energy when shined by a constant power but different wavelengths: Compared to that of photons with relatively low energy, photons with higher energy usually have high possibility to overcome the energy barriers, and contribute to the photocurrent. However, the increase of the photon energy is inevitably at the cost of photon number. As a consequence, the increase of incident photons can compensate the decrease of the possibility for the excited electron–hole pairs to become the effective photoinduced current. In this study, the photocurrent reaches the maximum value at 650 nm. A slight deviation in this wavelength will lead to less-efficient trade-off and therefore a low photocurrent will occur.^{28–30}

It is also revealed that the photoresponse of the CsBi₃I₁₀-film-based RLPD is dependent on the light intensity. Figure 4a shows the I - V characteristics under 650 nm light illumination, with light intensity ranging from 27.8 μ W/cm² to 98.3 mW/cm². Apparently, under different intensities, the CsBi₃I₁₀-film-

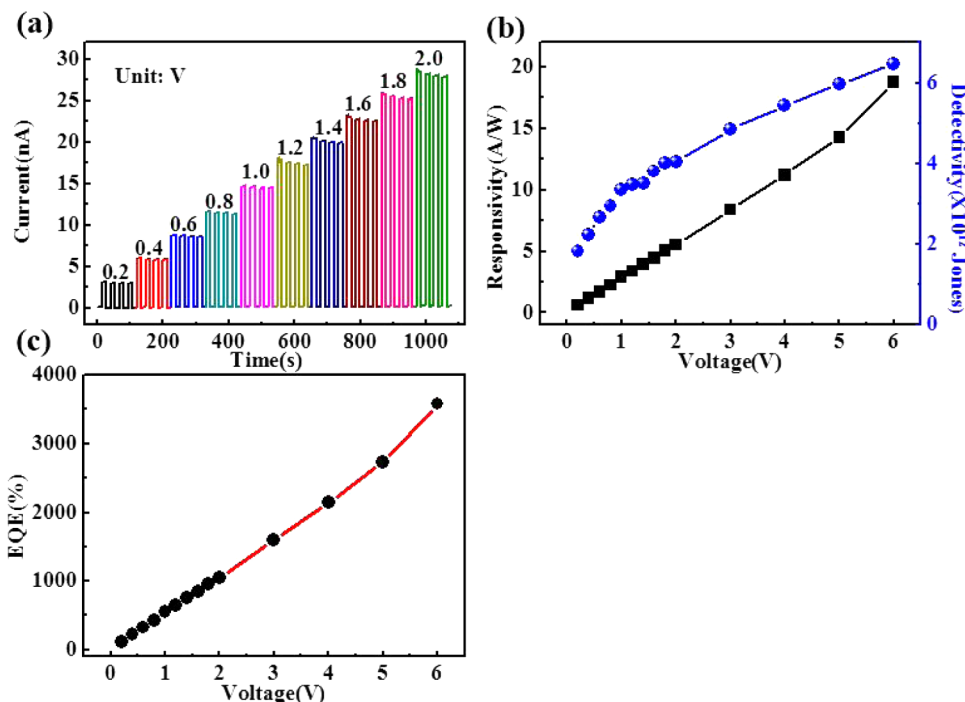


Figure 5. (a) Photocurrent of the RLPD under 650 nm light illumination at various bias voltages. (b) Responsivity and specific detectivity of the RLPD at different bias voltages. (c) EQE as a function of bias voltage.

based RLPD always exhibited a typical Ohmic contact. Furthermore, the photocurrent is found to gradually increase with increasing light intensity. Further study shows that such RLPD has an excellent switching characteristic: The photocurrent increases dramatically and stabilizes at an “on” state when shined by either strong or weak light illumination, but it decreases fast to an “off” state once the illumination was switched off. The rising edge and fall edge are very sharp, indicative of a very high response speed. A quantitative study of the light-intensity-dependent photocurrent demonstrates that the photocurrent can be roughly described by a power law: $I = AP^\theta$, where I is the current under light illumination, A is a constant of 650 nm, P is the intensity of the red light, and θ is an exponent. By fitting the experimental results shown in Figure 4c, the exponent θ is determined to be 0.99 for this CsBi₃I₁₀-film-based RLPD. This exponent, which is very close to 1, confirms that the perovskite film is of high quality with a relatively low density of defect states.³¹ To quantitatively compare the device performance of the present RLPD to that of other perovskite-based photodetectors, the responsivity (R) and specific detectivity (D^*) were calculated as follows^{32,33}

$$R = \frac{I_\lambda - I_d}{P_\lambda S} \quad (1)$$

$$D^* = \frac{R_\lambda S^{1/2}}{(2eI_d)^{1/2}} \quad (2)$$

where I_λ is the photocurrent, I_d is the dark current, P_λ is the incident light intensity, S is the effective area of light irradiation ($S = 6 \times 10^{-8} \text{ m}^2$), and e is the value of electronic charge. According to the above equations and the experimental value ($I_\lambda = 2.62 \times 10^{-10} \text{ A}$, $I_d = 2.38 \times 10^{-13} \text{ A}$, $P_\lambda = 2 \times 10^{-4} \text{ W/cm}^2$), R_λ and D^* were estimated to be 21.8 A/W and 1.93×10^{13} Jones, respectively, at the bias voltage of 1 V. Figure 4d plots both R and D^* under various intensities of incident 650

nm light. One can see that both the responsivity and specific detectivity decrease with the increase of light intensity at weak light illumination. Furthermore, both these parameters keep nearly constant values when the light intensity is in the range of 10.7–100 mW/cm². Meanwhile, the EQE, which is the number of electrons probed per incident photon, can be estimated by $\text{EQE} = hcR_\lambda/e\lambda$, where h is Planck's constant, c is the velocity of the incident light, R_λ is the responsivity of the photodetector, e is the electronic charge, and λ is the wavelength of the incident light. Figure 4e plots the EQE at a bias voltage of 1 V; the EQE was as high as $4.13 \times 10^3\%$ at 0.2 mW/cm². This parameter displays almost the same evolution as responsivity and specific detectivity, as shown in Figure 4d. This saturation at a high light intensity was believed to be associated with the photocurrent saturation, which is due to the filling mechanism of the sensitizing centers of the CsBi₃I₁₀ film at high light intensity.^{34,35}

In addition to light intensity, the photocurrent of the RLPD was dependent on the bias voltage. Figure 5a shows the photocurrent at various bias voltages under the same illumination (wavelength = 650 nm, light intensity = 84.0 mW/cm²). In the bias voltage range of 0.2–6 V, the photocurrent gradually increases with bias voltage. To unveil how and to what extent the bias voltage will influence the responsivity, detectivity, and EQE, these three parameters corresponding to different bias voltages were calculated. As shown in Figure 5b,c, all of the three parameters increase gradually with increasing bias voltage. This finding is reasonable considering the fact that the high bias voltage will accelerate the transit of the photogenerated charges. Subsequently, the conductivity of the CsBi₃I₁₀ film was increased, leading to an increase in responsivity, specific detectivity, and EQE.³⁶

Next, the photoresponse to pulsed illumination was studied. The equivalent circuit and setup for the measurement is illustrated in Figure 6a, in which R_g is the photodetector and R_L

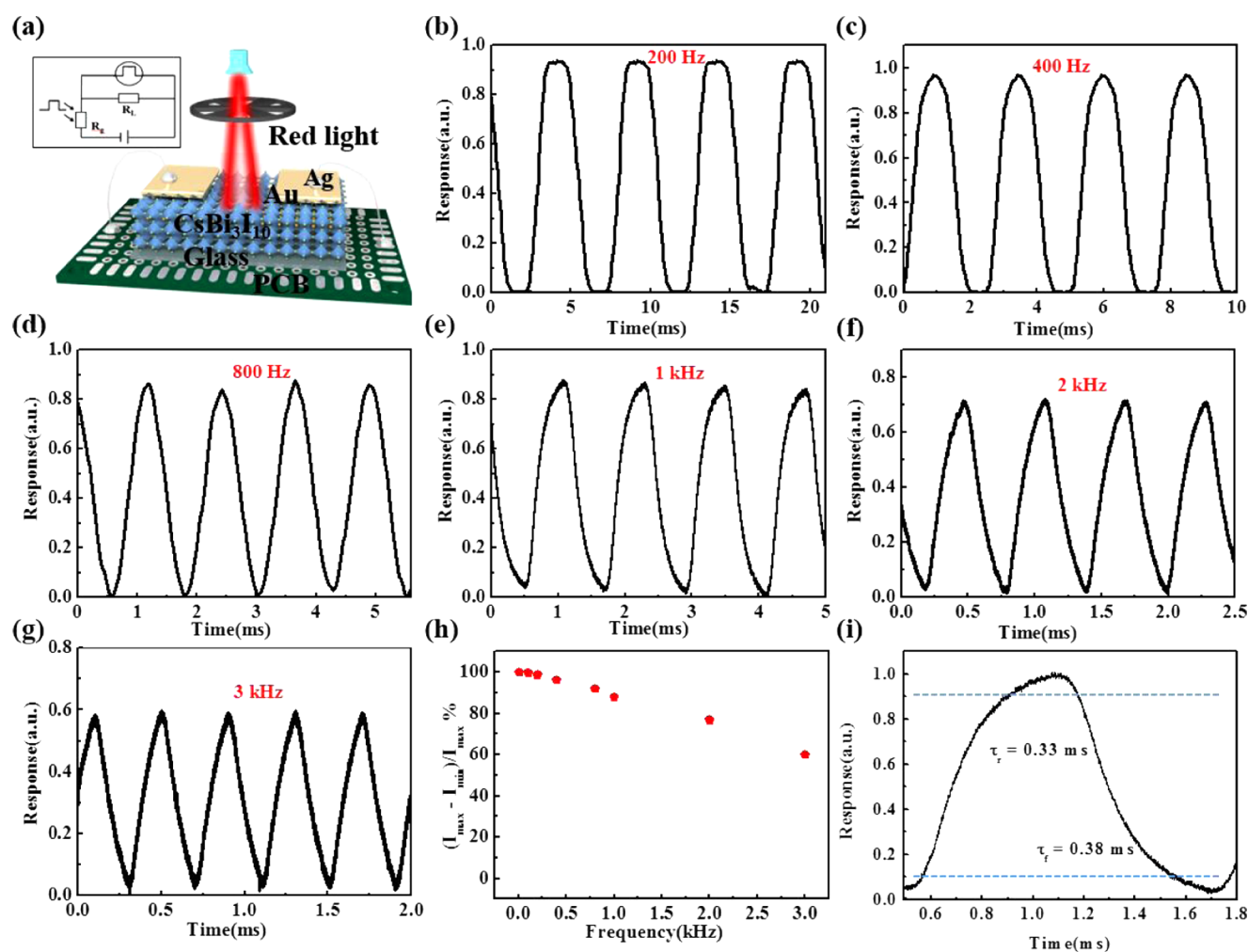


Figure 6. (a) Schematic illustration of the measurement setup. Photoresponse of the RLPD under pulsed red light with frequencies of (b) 200 Hz, (c) 400 Hz, (d) 800 Hz, (e) 1 kHz, (f) 2 kHz, and (g) 3 kHz. (h) $(I_{\max} - I_{\min})/I_{\max}$ vs switching frequency. (i) A single normalized cycle of the RLPD for estimating both rise time and fall time.

Table 1. Comparison of Device Performance of the Present RLPD to That of Other Perovskite-Material-Based Photodetectors

device structure	responsivity (A/W)	τ_r/τ_f (ms)	on/off ratio	ref
CsBi ₃ I ₁₀ film	21.8	0.33/0.38	10 ⁵	this work
MAPbI ₃ nanoparticles	3.49	100/100	152	18
CH ₃ NH ₃ SnI ₃ nanowire arrays	0.47	1500/400	>5	22
(CH ₃ NH ₃) ₂ MnCl ₄ thin film			120	23
CsPbBr ₃ nanosheets/CNTs	31.1	0.016/0.38	10 ⁵	37
(RNH ₃) ₂ (CH ₃ NH ₃) _{n-1} M _n X _{3n+1}	0.013	10/7.5	10 ³	38
CsPbBr ₃ microparticles	0.18	1.8/1.0	8 × 10 ³	39
MAPbI ₃ nanowires	1.32	0.3/0.3	23	40
MAPbI ₃ microwires	13.5	0.08/0.24	~10 ³	41
MAPbI ₃ nanowires	0.005	0.5/0.5	300	42
MAPbI ₃ (network)	0.1	0.3/0.4	300	43
TiO ₂ -MAPbI ₃	0.00049	20/20		44
CsPbBr ₃ nanoparticles/Au NCs	0.01	0.2/1.2		45
WS ₂	0.7	4100/4400		46
Mo _{0.5} W _{0.5} S ₂ alloy films	5.8	<150		47
Bi ₂ Te ₃ -Si	1	<100		48
PbS NC/Ag NC	0.004			49

is a series resistor with a resistance of 80 MΩ. Figure 6b–g shows the photoresponse of the RLPD under pulsed 650 nm light irradiation with various frequencies of 200 Hz, 400 Hz, 800 Hz, 1 kHz, 2 kHz, and 3 kHz, respectively. Apparently, the

device could be repeatedly switched between on and off states. Specifically, Figure 6h shows that the relative balance $[(I_{\max} - I_{\min})/I_{\max}]$ of the RLPD was still larger than 60% when the switching frequency was as high as 3 kHz, indicative of the great

potential of the RLPD for sensing fast-switching optical signals. According to the normalized cycle of photoresponse under 3 kHz light illumination, rise time (τ_r) and fall time (τ_f), corresponding to the time from 10 to 90% and from 90 to 10%, respectively, were determined to be 0.33 and 0.38 ms, respectively. Table 1 compares the responsivity, response time, and on/off ratio of the present RLPD to those of other perovskite-film-based devices. It is evident from the table that these three parameters of our device are poorer than those of the photodetector made of CsPbBr₃ nanosheets/carbon nanosheets (CNTs).³⁷ However, these values are much better than those of the other devices listed in the table, including MAPbI₃ (nanoparticles,¹⁸ nanowire,^{40,42} microwire,⁴¹ network,⁴³ and heterojunction⁴⁴), CsPbBr₃ (microparticles,³⁹ nanoparticles⁴⁵), CH₃NH₃SnI₃ nanowire,²² (CH₃NH₃)₂MnCl₄ thin film,²³ (RNH₃)₂(CH₃NH₃)_{n-1}M_nX_{3n+1},³⁸ and so on. In addition to that of the perovskite-material-based photodetectors, the performance of the present RLPD is better than that of other chalcogenide semiconductor devices made of WS₂,⁴⁶ Mo_{0.5}W_{0.5}S₂ alloy films,⁴⁷ Bi₂Te₃-Si heterojunction,⁴⁸ and PbS NC/Ag NC hybrid structure.⁴⁹

Another outstanding merit of the present RLPD is its excellent device stability. Figure 7a plots the photoresponse of

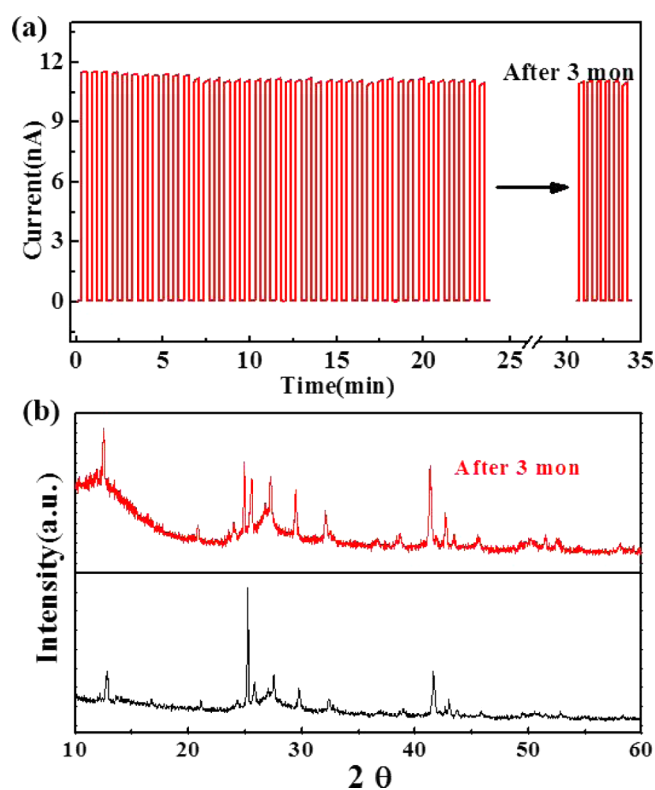


Figure 7. (a) Photoresponse of the RLPD for 40 cycles; the last five cycles correspond to the photoresponse after storage in air for 3 months. (b) Comparison of the XRD pattern of the CsBi₃I₁₀ film before and after 3 months.

the RLPD for 40 cycles under ambient condition. It can be seen that the response is very stable, with nearly identical photocurrent and dark current for each cycle. Remarkably, this device showed excellent stability after storage for 3 months, without any encapsulation and protection, as opposed to previously reported methylammonium lead halide-based devices,^{39,50,51} which normally suffer from poor device stability.

Understandably, such a good ambient stability is associated with the special inorganic structure, in which the substitution of methylammonium with an inorganic cesium atom can endure long-time exposure to ambient condition and therefore substantially increase the material stability. In fact, the good stability is also confirmed by XRD patterns before and after 3 months. As illustrated in Figure 7b, all of the peaks attributed to the CsBi₃I₁₀ film in the XRD pattern keep virtually unchanged after long-term storage, except some slight variation in the peak intensity. This excellent device stability, together with the good device performance will render the present RLPD potentially useful for the assembly of high-performance optoelectronic systems in future.

CONCLUSIONS

In this study, we report on the fabrication of nontoxic, lead-free, inorganic CsBi₃I₁₀ perovskite film for RLPD application. The as-fabricated perovskite device exhibited high sensitivity to red light, with excellent reproducibility, good spectral selectivity, and a high on/off ratio of 10⁵. The responsivity and specific detectivity were as high as 21.8 A/W and 1.93 × 10¹³ Jones, respectively. It was also found that the perovskite photodetector is capable of detecting pulsed light illumination with a frequency as high as 3 kHz. Furthermore, the rise and fall times were estimated to be 0.33 and 0.38 ms, respectively. These excellent device parameters and the good device stability under ambient condition corroborate that this CsBi₃I₁₀-perovskite-based photodetector has great promise for future optoelectronic device application.

EXPERIMENTAL SECTION

Materials Preparation and Characterization. In this study, the CsBi₃I₁₀ film was synthesized using a precursor, which was grown by a modified method.²⁵ All chemicals were purchased and used without further purification (BiI₃, 99.99%, Macklin Company; CsI, 99.9%, Macklin Company). Briefly, 0.2598 g of CsI and 1.7691 g of BiI₃ were dissolved in a mixed solvent (1 mL) containing DMF and DMSO with a volume ratio of 13:1. The resulting solution was filtered by a poly(tetrafluoroethylene) filter paper heated up to 70 °C for 10 min before use. To fabricate the CsBi₃I₁₀ film, a glass plate (1 cm × 1 cm) was washed with acetone, ethyl alcohol, and ultrapure water for 15 min, respectively. After treating in oxygen plasma for 12 min, the glass plate was spin-coated with the precursor solution at 3000 rpm for 60 s, followed by rinsing with 1 mL of chloroform (CHCl₃). The as-deposited sample was then dried in vacuum at 125 °C for 30 min to improve crystal property and further allowed to cool to room temperature. The brownish black CsBi₃I₁₀ perovskite film was characterized by FESEM (SIRION 200 FEG) and an X-ray diffractometer (Rigaku D/Max-rB).

Device Fabrication and Analysis. To fabricate the RLPD device, the above CsBi₃I₁₀ perovskite film with a homemade shadow mask was put into the chamber of an ultrahigh vacuum electron-beam evaporator (6.7 × 10⁻³ Pa), which will be used to deposit two parallel Au electrodes (50 nm) on both sides. The optoelectronic property of the CsBi₃I₁₀-film-based RLPD was examined by an *I*-*V* semiconductor characterization system (4200-SCS; Keithley Co. Ltd) equipped with a monochromator (SP2150; Princeton Co.), from which the monochromatic light was directly focused and guided onto the RLPD. To measure the response speed of the RLPD to pulsed light, a homemade setup composed of a 650 nm laser diode (Q-Line, P-200mW-A), driven by a signal generator, and an oscilloscope (TDS2012B; Tektronix) was used. Before device analysis, the power intensity of the incident light was calibrated by a powermeter (Thorlabs GmbH, PM 100D).

AUTHOR INFORMATION

Corresponding Authors

*E-mail: jmzhu@hfnu.edu.cn (J.-M.Z.).

*E-mail: luolb@hfnu.edu.cn (L.-B.L.).

*E-mail: zhwang@mail.ahnu.edu.cn (Z.-H.W.).

ORCID

Lin-Bao Luo: 0000-0001-8651-8764

Zheng-Hua Wang: 0000-0002-1073-8055

Notes

The authors declare no competing financial interest.

ACKNOWLEDGMENTS

This study was supported by the National Natural Science Foundation of China (NSFC Nos. 21671007, 61575059, and 21501038) and the Fundamental Research Funds for the Central Universities (2013HGCH0012 and 2014HGCH0005).

REFERENCES

- (1) Kojima, A.; Teshima, K.; Shirai, Y.; Miyasaka, T. Organometal Halide Perovskites as Visible-Light Sensitizers for Photovoltaic Cells. *J. Am. Chem. Soc.* **2009**, *131*, 6050–6051.
- (2) Li, Y.; Meng, L.; Yang, Y. M.; Xu, G. Y.; Hong, Z. R.; Chen, Q.; You, J. B.; Li, G.; Yang, Y.; Li, Y. High-Efficiency Robust Perovskite Solar Cells on Ultrathin Flexible Substrates. *Nat. Commun.* **2016**, *7*, No. 10214.
- (3) Shi, D.; Adinolfi, V.; Comin, R.; Yuan, M. J.; Alarousu, E.; Buin, A.; Chen, Y.; Hoogland, S.; Rothenberger, A.; Katsiev, K.; Losovyj, Y.; Zhang, X.; Dowben, P. A.; Mohammed, O. F.; Sargent, E. H.; Bakr, O. M. Low Trap-State Density and Long Carrier Diffusion in Organolead Trihalide Perovskite Single Crystals. *Science* **2015**, *347*, 519–522.
- (4) Zhu, P.; Gu, S.; Shen, X. P.; Xu, N.; Tan, Y. L.; Zhuang, S. D.; Deng, Y.; Lu, Z. D.; Wang, Z. L.; Zhu, J. Direct Conversion of Perovskite Thin Films into Nanowires with Kinetic Control for Flexible Optoelectronic Devices. *Nano Lett.* **2016**, *16*, 871–876.
- (5) Saidaminov, M. I.; Adinolfi, V.; Comin, R.; Abdelhady, A. L.; Peng, W.; Dursun, I.; Yuan, M. J.; Hoogland, S.; Sargent, E. H.; Bakr, O. M. Planar-integrated Single-Crystalline Perovskite Photodetectors. *Nat. Commun.* **2015**, *6*, No. 8724.
- (6) Zhou, J.; Chu, Y. L.; Huang, J. Photodetectors Based on Two-Dimensional Layer-Structured Hybrid Lead Iodide Perovskite Semiconductors. *ACS Appl. Mater. Interfaces* **2016**, *8*, 25660–25666.
- (7) Wang, F.; Mei, J. J.; Wang, Y. P.; Zhang, L. G.; Zhao, H. F.; Zhao, D. X. Fast Photoconductive Responses in Organometal Halide Perovskite Photodetectors. *ACS Appl. Mater. Interfaces* **2016**, *8*, 2840–2846.
- (8) Wang, Z.; Yu, R. M.; Pan, C. F.; Li, Z. L.; Yang, J.; Yi, F.; Wang, Z. L. Light-Induced Pyroelectric Effect as An Effective Approach for Ultrafast Ultraviolet Nanosensing. *Nat. Commun.* **2015**, *6*, No. 8401.
- (9) Deng, W.; Zhang, X. J.; Huang, L. M.; Xu, X. Z.; Wang, L.; Wang, J. C.; Shang, Q. X.; Lee, S. T.; Jie, J. S. Aligned Single-Crystalline Perovskite Microwire Arrays for High-Performance Flexible Image Sensors with Long-Term Stability. *Adv. Mater.* **2016**, *28*, 2201–2208.
- (10) Pan, J.; Quan, L. N.; Zhao, Y.; Peng, W.; Murali, B.; Sarmah, S. P.; Yuan, M.; Sinatra, L.; Alyami, N. M.; Liu, J.; Yassitepe, E.; Yang, Z.; Voznyy, O.; Comin, R.; Hedhili, M. N.; Mohammed, O. F.; Lu, Z. H.; Kim, D. H.; Sargent, E. H.; Bakr, O. M. Highly Efficient Perovskite-Quantum-Dot Light-Emitting Diodes by Surface Engineering. *Adv. Mater.* **2016**, *28*, 8718–8725.
- (11) Wong, A. B.; Lai, M. L.; Eaton, S. W.; Yu, Y.; Lin, E.; Dou, L. T.; Fu, A.; Yang, P. D. Growth and Anion Exchange Conversion of $\text{CH}_3\text{NH}_3\text{PbX}_3$ Nanorod Arrays for Light-Emitting Diodes. *Nano Lett.* **2015**, *15*, 5519–5524.
- (12) Jaramillo-Quintero, O. A.; Sanchez, R. S.; Rincon, M.; Mora-Sero, I. Bright Visible-Infrared Light Emitting Diodes Based on Hybrid Halide Perovskite with Spiro-OMeTAD as A Hole-Injecting Layer. *J. Phys. Chem. Lett.* **2015**, *6*, 1883–1890.
- (13) Deng, W.; Xu, X. Z.; Zhang, X. J.; Zhang, Y. D.; Jin, X. C.; Wang, L.; Lee, S. T.; Jie, J. S. Organometal Halide Perovskite Quantum Dot Light-Emitting Diodes. *Adv. Funct. Mater.* **2016**, *26*, 4797–4802.
- (14) Veldhuis, S. A.; Boix, P. P.; Yantara, N.; Li, M. J.; Sum, T. C.; Mathews, N.; Mhaisalkar, S. G. Perovskite Materials for Light-Emitting Diodes and Lasers. *Adv. Mater.* **2016**, *28*, 6804–6834.
- (15) Zhu, H.; Fu, Y. P.; Meng, F.; Wu, X. X.; Gong, Z. Z.; Ding, Q.; Gustafsson, M. V.; Trinh, M. T.; Jin, S.; Zhu, X.-Y. Lead Halide Perovskite Nanowire Lasers with Low Lasing Thresholds and High Quality Factors. *Nat. Mater.* **2015**, *14*, 636–642.
- (16) Zhang, Q.; Ha, S. T.; Liu, X. F.; Sum, T. C.; Xiong, Q. H. Room-Temperature Near-Infrared High-Q Perovskite Whispering-Gallery Planar Nano Lasers. *Nano Lett.* **2014**, *14*, 5995–6001.
- (17) Lee, Y.; Kwon, J.; Hwang, E.; Ra, C.-H.; Yoo, W. J.; Ahn, J.-H.; Park, J. H.; Cho, J. H. High-Performance Perovskite-Graphene Hybrid Photodetector. *Adv. Mater.* **2015**, *27*, 41–46.
- (18) Hu, X.; Zhang, X. D.; Liang, L.; Bao, J.; Li, S.; Yang, W. L.; Xie, Y. High-Performance Flexible Broadband Photodetector Based on Organolead Halide Perovskite. *Adv. Funct. Mater.* **2014**, *24*, 7373–7380.
- (19) Dou, L.; Yang, Y.; You, J. B.; Hong, Z. R.; Chang, W.-H.; Li, G.; Yang, Y. Solution-Processed Hybrid Perovskite Photodetectors with High Detectivity. *Nat. Commun.* **2014**, *5*, No. 5404.
- (20) Krishnamoorthy, T.; Ding, H.; Yan, C.; Leong, W. L.; Baikie, T.; Zhang, Z. Y.; Sherburne, M.; Li, S. Z.; Asta, M.; Mathews, N.; Mhaisalkar, S. G. Lead-Free Germanium Iodide Perovskite Materials for Photovoltaic Applications. *J. Mater. Chem. A* **2015**, *3*, 23829–23832.
- (21) Parobek, D.; Roman, B. J.; Dong, Y. T.; Jin, H.; Lee, E.; Sheldon, M.; Son, D. H. Exciton-to-Dopant Energy Transfer in Mn-Doped Cesium Lead Halide Perovskite Nanocrystals. *Nano Lett.* **2016**, *16*, 7376–7380.
- (22) Waleed, A.; Tavakoli, M. M.; Gu, L. L.; Wang, Z. Y.; Zhang, D. Q.; Manikandan, A.; Zhang, Q. P.; Zhang, R. J.; Chueh, Y.-L.; Fan, Z. Y. Lead-Free Perovskite Nanowire Array Photodetectors with Drastically Improved Stability in Nanoengineering Templates. *Nano Lett.* **2017**, *17*, 523–530.
- (23) Nie, Z.; Yin, J.; Zhou, H. W.; Chai, N.; Chen, B. L.; Zhang, Y. T.; Qu, K. G.; Shen, G. D.; Ma, H. Y.; Li, Y. C.; Zhao, J. S.; Zhang, X. X. Layered and Pb-Free Organic-Inorganic Perovskite Materials for Ultraviolet Photoresponse: (010)-Oriented $(\text{CH}_3\text{NH}_3)_2\text{MnCl}_4$ Thin Film. *ACS Appl. Mater. Interfaces* **2016**, *8*, 28187–28193.
- (24) Babayigit, A.; Ethirajan, A.; Muller, M.; Conings, B. Toxicity of Organometal Halide Perovskite Solar Cells. *Nat. Mater.* **2016**, *15*, 247–251.
- (25) Johansson, M. B.; Zhu, H. M.; Johansson, E. M. J. Extended Photo-Conversion Spectrum in Low-Toxic Bismuth Halide Perovskite Solar Cells. *J. Phys. Chem. Lett.* **2016**, *7*, 3467–3471.
- (26) Cho, H.; Jeong, S. H.; Park, M.-H.; Kim, Y.-H.; Wolf, C.; Lee, C. L.; Heo, J. H.; Sadhanala, A.; Myoung, N.; Yoo, S.; Im, S. H.; Friend, R. H.; Lee, T. W. Overcoming the Electroluminescence Efficiency Limitations of Perovskite Light-Emitting Diodes. *Science* **2015**, *350*, 1222–1225.
- (27) Li, X.; Bi, D. Q.; Yi, C. Y.; Decoppet, J. D.; Luo, J. S.; Zakeeruddin, S. M.; Hagfeldt, A.; Gratzel, M. A Vacuum Flash-Assisted Solution Process for High-Efficiency Large-Area Perovskite Solar Cells. *Science* **2016**, *353*, 58–62.
- (28) Yao, J.; Deng, Z. X.; Zheng, Z. Q.; Yang, G. W. Stable, Fast UV-Vis-NIR Photodetector with Excellent Responsivity, Detectivity, and Sensitivity Based on $\alpha\text{-In}_2\text{Te}_3$ Films with a Direct Bandgap. *ACS Appl. Mater. Interfaces* **2016**, *8*, 20872–20879.
- (29) Rose, A. *Concepts in Photoconductivity and Allied Problems*; Krieger: New York, 1978.
- (30) Yao, J. D.; Shao, J. M.; Yang, G. W. Ultra-Broadband and High-Responsive Photodetector Based on Bismuth Film at Room Temperature. *Sci. Rep.* **2015**, *5*, No. 12320.
- (31) Zeng, L. H.; Wang, M. Z.; Hu, H.; Nie, B.; Yu, Y. Q.; Wu, C. Y.; Wang, L.; Hu, J. G.; Xie, C.; Liang, F. X.; Luo, L. B. Monolayer

Graphene/Germanium Schottky Junction As High-Performance Self-Driven Infrared Light Photodetector. *ACS Appl. Mater. Interfaces* **2013**, *5*, 9362–9366.

(32) Liu, J. M. *Photonic Devices*; Cambridge University Press: Cambridge, 2005.

(33) Luo, L. B.; Chen, J. J.; Wang, M. Z.; Hu, H.; Wu, C. Y.; Li, Q.; Wang, L.; Huang, J. A.; Liang, F. X. Near-Infrared Light Photovoltaic Detector Based on GaAs Nanocone Array/Monolayer Graphene Schottky Junction. *Adv. Funct. Mater.* **2014**, *24*, 2794–2800.

(34) Bube, R. H.; Ho, C. T. Laser Saturation of Photoconductivity and Determination of Imperfection Parameters in Sensitive Photoconductors. *J. Appl. Phys.* **1966**, *37*, 4132–4138.

(35) Domanski, K.; Tress, W.; Moehl, T.; Saliba, M.; Nazeeruddin, M. K.; Graetzel, M. Working Principles of Perovskite Photodetectors: Analyzing the Interplay Between Photoconductivity and Voltage-Driven Energy-Level Alignment. *Adv. Funct. Mater.* **2015**, *25*, 6936–6947.

(36) Kong, W. Y.; Wu, G. A.; Wang, K. Y.; Zhang, T. F.; Zou, Y. F.; Wang, D. D.; Luo, L. B. Graphene-beta-Ga₂O₃ Heterojunction for Highly Sensitive Deep UV Photodetector Application. *Adv. Mater.* **2016**, *28*, 10725–10731.

(37) Li, X.; Yu, D. J.; Chen, J.; Wang, Y.; Cao, F.; Wei, Y.; Wu, Y.; Wang, L.; Zhu, Y.; Sun, Z. G.; Ji, J. P.; Shen, Y. L.; Sun, H. D.; Zeng, H. B. Constructing Fast Carrier Tracks into Flexible Perovskite Photodetectors To Greatly Improve Responsivity. *ACS Nano* **2017**, *11*, 2015–2023.

(38) Zhou, J.; Chu, Y. L.; Huang, J. Photodetectors Based on Two-Dimensional Layer-Structured Hybrid Lead Iodide Perovskite Semiconductors. *ACS Appl. Mater. Interfaces* **2016**, *8*, 25660–25666.

(39) Li, X. M.; Yu, D. J.; Cao, F.; Gu, Y.; Wei, Y.; Wu, Y.; Song, J. Z.; Zeng, H. B. Healing All-Inorganic Perovskite Films via Recyclable Dissolution-Recrystallization for Compact and Smooth Carrier Channels of Optoelectronic Devices with High Stability. *Adv. Funct. Mater.* **2016**, *26*, 5903–5912.

(40) Deng, H.; Dong, D. D.; Qiao, K. K.; Bu, L. L.; Li, B.; Yang, D.; Wang, H. E.; Cheng, Y. B.; Zhao, Z. X.; Tanga, J.; Song, H. S. Growth, Patterning and Alignment of Organolead Iodide Perovskite Nanowires for Optoelectronic Devices. *Nanoscale* **2015**, *7*, 4163–4170.

(41) Deng, W.; Zhang, X. J.; Huang, L. L.; Xu, X. Z.; Wang, L.; Wang, J. C.; Shang, Q. X.; Lee, S. T.; Jie, J. S. Aligned Single-Crystalline Perovskite Microwire Arrays for High-Performance Flexible Image Sensors with Long-Term Stability. *Adv. Mater.* **2016**, *28*, 2201–2208.

(42) Horváth, E.; Spina, M.; Szekrenyes, Z.; Kamaras, K.; Gaal, R.; Gachet, D.; Forro, L. Nanowires of Methylammonium Lead Iodide (CH₃NH₃PbI₃) Prepared by Low Temperature Solution-Mediated Crystallization. *Nano Lett.* **2014**, *14*, 6761–6766.

(43) Deng, H.; Yang, X. K.; Dong, D. D.; Li, B.; Yang, D.; Yuan, S. G.; Qiao, K. K.; Cheng, Y.-B.; Tang, J.; Song, H. S. Flexible and Semitransparent Organolead Triiodide Perovskite Network Photodetector Arrays with High Stability. *Nano Lett.* **2015**, *15*, 7963–7969.

(44) Xia, H. R.; Li, J.; Sun, W. T.; Peng, L. M. Organohalide Lead Perovskite Based Photodetectors with Much Enhanced Performance. *Chem. Commun.* **2014**, *50*, 13695–13697.

(45) Dong, Y.; Gu, Y.; Zou, Y. S.; Song, J. Z.; Xu, L. M.; Li, J. H.; Xue, F.; Li, X. M.; Zeng, H. B. Improving All-Inorganic Perovskite Photodetectors by Preferred Orientation and Plasmonic Effect. *Small* **2016**, *12*, 5622–5632.

(46) Yao, J. D.; Zheng, Z. Q.; Shao, J. M.; Yang, G. W. Stable, Highly-Responsive and Broadband Photodetection Based on Large-area Multilayered WS₂ Films Grown by Pulsed-Laser Deposition. *Nanoscale* **2015**, *7*, 14974–14981.

(47) Yao, J.; Zheng, Z. Q.; Yang, J. W. Promoting the Performance of Layered-Material Photodetectors by Alloy Engineering. *ACS Appl. Mater. Interfaces* **2016**, *8*, 12915–12924.

(48) Yao, J. D.; Shao, J. M.; Wang, Y. X.; Zhao, Z. R.; Yang, G. W. Ultra-Broadband and High Response of The Bi₂Te₃-Si Heterojunction and Its Application as A Photodetector at Room Temperature in Harsh Working Environments. *Nanoscale* **2015**, *7*, 12535–12541.

(49) Saran, R.; Curry, R. J. Lead Sulphide Nanocrystal Photodetector Technologies. *Nat. Photonics* **2016**, *10*, 81–92.

(50) Xiao, Z.; Yuan, Y. B.; Shao, Y. H.; Wang, Q.; Dong, Q. F.; Bi, C.; Sharma, P.; Gruverman, A.; Huang, J. S. Giant Switchable Photovoltaic Effect in Organometal Trihalide Perovskite Devices. *Nat. Mater.* **2015**, *14*, 193–198.

(51) Wang, Y.; Xia, Z. G.; Du, S. N.; Yuan, F.; Li, Z. G.; Li, Z. J.; Dai, Q.; Wang, H. L.; Luo, S. Q.; Zhang, S. D.; Zhou, H. Solution-Processed Photodetectors Based on Organic-Inorganic Hybrid Perovskite and Nanocrystalline Graphite. *Nanotechnology* **2016**, *27*, No. 175201.